Composite Structures 164 (2017) 237–247

Contents lists available at ScienceDirect

Composite Structures

journal homepage: www.elsevier.com/locate/compstruct

Post-cure shape errors of ultra-thin symmetric CFRP laminates: Effect of ply-level imperfections

John Steeves [a,*], Sergio Pellegrino [b]

[a] Jet Propulsion Laboratory, California Institute of Technology, 4800 Oak Grove Dr, Pasadena, CA 91109, United States
[b] California Institute of Technology, 1200 E. California Blvd, Pasadena, CA 91125, United States

ARTICLE INFO

Article history:
Received 10 August 2016
Revised 10 December 2016
Accepted 27 December 2016
Available online 29 December 2016

Keywords:
Thin-ply composites
CFRP
Cross-ply
Imperfections
Shape errors

ABSTRACT

This paper discusses the effect of misalignments in ply orientation, uniform variations in ply thickness, and through-thickness thermal gradients on the post-cure shape errors for symmetric cross-ply laminates constructed from ultra-thin composite materials. Photogrammetry-based surface measurements are performed for laminates cured at elevated temperatures. Significant out-of-plane shape errors are observed, with amplitudes ~75 times the laminate thickness. The magnitude of each imperfection is also characterized experimentally on coupon-level samples. A non-linear finite element model is developed and demonstrates that these imperfections result in cylindrical and twisting modes of deformation. Results are compared to Classical Lamination Theory predictions which are shown to be inadequate in predicting shape errors that require changes in Gaussian curvature. Through these studies, it is determined that thickness variations between the top and bottom plies have the most pronounced effect on shape errors.

© 2017 Elsevier Ltd. All rights reserved.

1. Introduction

Advancements in tow-spreading techniques have allowed the production of ultra-thin unidirectional carbon fiber prepreg materials [1–3]. In the context of this study, "ultra-thin" refers to individual ply thicknesses on the order of 20–30 μm, with fiber areal weights (FAWs) down to 17 gsm. The benefits of using such materials have recently been studied, demonstrating increased mechanical performance over traditional composite materials [1,4–7].

By using ultra-thin laminas, symmetric multi-ply laminates with quasi-isotropic properties can be constructed while keeping the overall laminate thickness extremely low (<200 μm). These laminates are ideal for structures requiring high levels of compliance in bending, such as hingeless deployable structures [8–11] as well as structures with low areal densities, such as lightweight mirrors and reflectors [12,13]. Many of these applications pose stringent requirements on surface accuracy. Therefore, the questions to be answered are: is it possible to manufacture precision shell/plate structures at such low laminate thicknesses, and what are the precision limits that can be achieved?

Fiber-reinforced laminates develop significant internal stresses when cooled from their elevated cure temperature. These stresses arise due to the highly orthotropic nature of the individual plies. Specifically, large differences in stiffness and coefficient of thermal expansion (CTE) in the directions aligned with and perpendicular to the fiber direction can cause the laminate to warp after cure. However, if the laminate orientation is made symmetric with respect to the mid-plane, and the curing conditions are uniform over the entire part, it is normally accepted that these cool-down stresses will balance through the thickness and zero out-of-plane deformations will occur. Hence, if cured on a flat surface under these ideal conditions, the laminate should remain flat. However, even small deviations from this ideal case can break the intended laminate symmetry, creating an imbalance in the thermal stresses and ultimately result in the presence of post-cure shape errors.

Symmetry-breaking imperfections can be caused by errors in the relative orientation of successive plies, which break the intended symmetry of a laminate. Hinckley [14] performed Monte Carlo analyses to assess the effect of ply misalignment on mechanical and thermal properties, and for various laminate orientations. Recommendations on lay-up and stacking processes were made in order to reduce thermally induced warping. Arao [15] assessed the effect of ply misalignment due to moisture absorption for symmetric laminates, a relatively similar problem to the present. Significant twisting deformations were predicted in spite of the nominally symmetric laminate orientation. Fiber waviness within

* Corresponding author.
E-mail address: john.b.steeves@jpl.nasa.gov (J. Steeves).

http://dx.doi.org/10.1016/j.compstruct.2016.12.075
0263-8223/© 2017 Elsevier Ltd. All rights reserved.

a ply can also create variations in the effective ply orientation making it impossible to construct a perfectly symmetric laminate. Studies have been performed in order to characterize the magnitude of fiber waviness in a ply [16,17], and it was found that waviness introduces significant variability in mechanical and thermal properties [18–22]. However, the experimental investigations in these studies were conducted on samples with thicknesses greater than 1.0 mm and little information is available for ultra-thin materials.

Variation in the through-thickness distribution of fibers within the plies has also been shown to be important, since deviations in fiber volume fraction up to 10% have been observed experimentally [23]. Additionally, variations in the curing conditions of laminates can also result in the development of post-cure shape errors. Efforts to model these effects, by predicting the temperature distribution and resin cure progression throughout the thermal process have shown that thermal gradients during curing can produce large out-of-plane deformations [24,25].

The present study focuses on post-cure shape errors in laminates constructed from ultra-thin carbon-fiber reinforced polymer (CFRP) materials, caused by misalignments in the orientation of each ply, uniform variations in the mean thickness of each ply, and through-thickness thermal gradients during the curing process. Four-ply symmetric laminates are considered. Each ply has a nominal thickness of 20 μm and therefore the total thickness of the laminate is only 80 μm. This represents a factor of 5–10 reduction in thickness over traditional composite laminates.

The paper is structured as follows: Section 2 presents a linear analysis using Classical Lamination Theory (CLT) to assess the effect of the above imperfections on post-cure shape errors. Section 3 describes the experiments that were carried out. Full-field shape measurements of three cured samples are presented along with a preliminary characterization of the imperfections at the coupon level. Section 4 presents a non-linear finite element model used to simulate the cool-down process after cure. Predictions of shape errors are made for each imperfection occurring independently, and are then compared against CLT predictions. A sensitivity analysis that compares the relative effect of each imperfection is also presented along with a specific example for comparison to the experiments. Finally, Section 5 discusses the results and concludes the paper.

2. Preliminary analysis

It is well known that Classical Lamination Theory (CLT) [26] can be used to predict the mid-plane strains and out-of-plane curvature changes of a laminate under the assumptions of geometric and material linearity. Given a laminate constructed from n separate plies, the 6×6 **ABD** stiffness matrix relates the mid-plane strains and out-of-plane curvatures, $\boldsymbol{\epsilon}$ and $\boldsymbol{\kappa}$, to the resultant forces and moments, **N** and **M**, respectively:

$$\begin{bmatrix} \boldsymbol{\epsilon} \\ \boldsymbol{\kappa} \end{bmatrix} = \begin{bmatrix} \mathbf{A} & \mathbf{B} \\ \mathbf{B} & \mathbf{D} \end{bmatrix}^{-1} \begin{bmatrix} \mathbf{N} \\ \mathbf{M} \end{bmatrix} \tag{1}$$

where

$$\mathbf{A} = \sum_{k=1}^{n} \mathbf{Q}_k (z_k - z_{k-1}), \tag{2}$$

$$\mathbf{B} = 1/2 \sum_{k=1}^{n} \mathbf{Q}_k (z_k^2 - z_{k-1}^2), \tag{3}$$

$$\mathbf{D} = 1/3 \sum_{k=1}^{n} \mathbf{Q}_k (z_k^3 - z_{k-1}^3). \tag{4}$$

$\mathbf{Q}_k$ is the orthotropic stiffness matrix of the kth ply in the laminate coordinate system (x, y), and z_k is the through-thickness interface coordinate of this ply and ply $k+1$, as shown in Fig. 1. $\mathbf{Q}_k$ is dependent on the material properties of the kth ply, as well as the orientation of the ply with respect to the laminate coordinate system. It has the expression

$$\mathbf{Q}_k = \mathbf{T}_k^{-1} \mathbf{Q}_k^{PMC} \mathbf{T}_k^{-T}, \tag{5}$$

where $\mathbf{Q}_k^{PMC}$ is the stiffness matrix of the kth ply in the prime material coordinate (PMC) system. The PMC system has axes parallel and perpendicular to the nominal fiber direction. $\mathbf{T}_k$ is a rotation matrix dependent on the ply orientation and is defined as

$$\mathbf{T}_k = \begin{bmatrix} c^2 & s^2 & 2cs \\ s^2 & c^2 & -2cs \\ -cs & cs & c^2 - s^2 \end{bmatrix} \tag{6}$$

with

$$s = \sin(\theta_k), \tag{7}$$

$$c = \cos(\theta_k), \tag{8}$$

where θ_k is the angle of the kth ply with respect to the x-axis.

For the present study, the mid-plane strains and out-of-plane curvatures produced after the laminate has been cured and then cooled to room-temperature are of interest. These are produced as a result of the internal thermal stresses developed during the cure. These stresses ultimately produce in-plane thermal forces and moments, $\mathbf{N}_T$ and $\mathbf{M}_T$, respectively, which have the expressions:

$$\mathbf{N}_T = \sum_{k=1}^{n} \int_{z_{k-1}}^{z_k} \mathbf{Q}_k \boldsymbol{\alpha}_k \Delta T dz, \tag{9}$$

$$\mathbf{M}_T = \sum_{k=1}^{n} \int_{z_{k-1}}^{z_k} \mathbf{Q}_k \boldsymbol{\alpha}_k \Delta T z dz, \tag{10}$$

where $\boldsymbol{\alpha}_k$ is the vector of in-plane thermal expansion coefficients for the kth ply in laminate coordinates and ΔT is the temperature change during cooling. $\boldsymbol{\alpha}_k$ also depends on the orientation of the fibers within a ply and is given by

$$\boldsymbol{\alpha}_k = \mathbf{R} \mathbf{T}^{-1} \mathbf{R}^{-1} \boldsymbol{\alpha}_k^{PMC}, \tag{11}$$

where $\boldsymbol{\alpha}_k^{PMC}$ is the vector of thermal expansion coefficients for the kth layer in the PMC system and $\mathbf{R} = \mathrm{diag}\{1, 1, 2\}$.

Substituting the thermal forces and moments into Eq. (1) gives

$$\begin{bmatrix} \boldsymbol{\epsilon} \\ \boldsymbol{\kappa} \end{bmatrix} = \begin{bmatrix} \mathbf{A} & \mathbf{B} \\ \mathbf{B} & \mathbf{D} \end{bmatrix}^{-1} \begin{bmatrix} \mathbf{N}_T \\ \mathbf{M}_T \end{bmatrix} \tag{12}$$

from which the out-of-plane curvatures produced during cure can be predicted.

It should be noted that this formulation makes several assumptions. Firstly, it is assumed that the laminate is unstressed after completion of the cure. Second, once cured the laminate is a linear elastic material with properties independent of temperature.

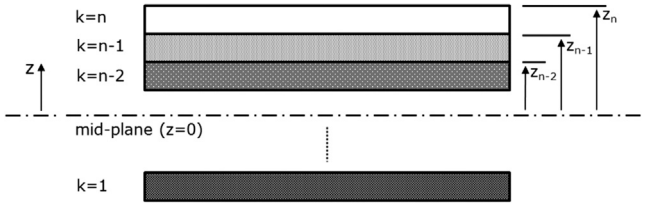

Fig. 1. Through-thickness coordinate definition for Classical Lamination Theory.

While the material viscoelasticity was neglected, the relaxation of the composite material at a ply level – characterized in Brinkmeyer et. al. (2016) [9] – will lead to decreases over time of both the bending stiffness and thermal moments, and hence the net result is expected to be small. Third, the laminate is unconstrained and therefore free to deform during cooling. These assumptions are known to be only partially valid for composite materials. For example, the thermal and mechanical properties of most polymeric resins are known to exhibit varying degrees of temperature dependency. Additionally, studies have been performed to investigate the thermo-mechanical interaction between composite laminates and the mandrel upon which they are cured [27,28]. Hence, although their validity is limited, these assumptions allow a preliminary investigation of the thermal deformations produced during cure and are a useful first step.

Using the formulation above, the conditions required to ensure that out-of-plane curvature changes do not arise during cooling of a laminate can be identified. Firstly, it is observed from Eq. (9) that the thermal forces are always non-zero during cool-down. However, if the **B** matrix is null, Eq. (12) can be reduced to

$$\begin{bmatrix} \boldsymbol{\epsilon} \\ \boldsymbol{\kappa} \end{bmatrix} = \begin{bmatrix} \mathbf{A}^{-1} & \mathbf{0} \\ \mathbf{0} & \mathbf{D}^{-1} \end{bmatrix} \begin{bmatrix} \mathbf{N}_T \\ \mathbf{M}_T \end{bmatrix} \tag{13}$$

and therefore, no coupling between out-of-plane curvatures, $\boldsymbol{\kappa}$, and resultant thermal forces, $\mathbf{N}_T$, will exist.

The first condition for **B = 0** is that opposing plies must possess identical stiffness matrices, $\mathbf{Q}_k$. Assuming identical properties in the PMC reference frame and from Eqs. (5) and (6) it follows that

$$\theta_k = \theta_{[n-(k-1)]}. \tag{14}$$

The second condition for **B = 0** is that plies opposite one another with respect to the laminate mid-plane must have identical thicknesses, t_k, hence

$$t_k = t_{[n-(k-1)]}, \tag{15}$$

with $k = 1, 2, \ldots, n/2$ for a laminate with an even ply count. Additionally, as $\mathbf{D} \neq \mathbf{0}$, there must be no thermal moments, $\mathbf{M}_T$, developed during the cure. From Eq. (10) it can be deduced that this condition is satisfied if perfectly symmetric lamination conditions exist and the laminate undergoes a uniform temperature change during cooling. In conclusion, opposing plies must have identical mechanical and thermal properties, fiber orientation, equal thicknesses, and ΔT must not be a function of the through-thickness coordinate for $\mathbf{M}_T = \mathbf{0}$.

Therefore, it follows that violation of each of these conditions through (1) variations in ply orientation, (2) variations in ply thickness, and (3) through-thickness thermal-gradients during cure, can result in out-of-plane deformations upon cooling.

3. Experiments

3.1. Preparation of test samples

Flat, square samples were prepared for this study. The samples were made flat such that simple tooling could be used and in order to avoid any issues related to prepreg draping. The square shape was chosen, because it provided straight edges that could be aligned with the fiber directions. Additionally, this geometry has the added benefit that it is 90° rotationally symmetric around an axis perpendicular to the square. Therefore, only one sample is required to study a specific laminate as there is no preferential alignment between the sample geometry and its laminate orientation. This would not be the case for rectangular samples, as the laminate will exhibit a different post-cure response if the terminal ply is aligned with or perpendicular to the long edge of the rectangle.

The composite material consisted of Toray T800H fibers embedded in a ThinPreg™ 120EPHTg-1 epoxy matrix. The material was obtained from North Thin Ply Technologies (NTPT) in prepreg form with a 38% resin content by weight. Each ply had a nominal fiber areal weight (FAW) of 17 gsm, corresponding to a nominal cured ply thickness of 20 μm. This material was chosen as it represented the thinnest commercially available unidirectional prepreg at the time of this study. The mechanical and thermal properties of this material were measured prior to the study and are listed in Table 1.

Two sets of laminates were constructed. The first set was used to study the shape errors produced after completion of the cure. These were four-ply laminates with a $[0°/90°]_s$ stacking orientation, chosen because it is the thinnest possible symmetric and balanced laminate. Three square laminates with a 250 mm side length were constructed. The samples were cured flat using a glass plate as the curing surface. A release agent, Loctite Frekote 700NC, was applied to the glass plate prior to laying up the laminate in order to aid release after the cure. A silicone pad was placed on top of the laminate to provide an even pressure distribution during the cure. While this pad did not allow for bleed-off of excess resin, it was necessary to achieve adequate thickness uniformity in the laminate during the cure. Attempts were made to use traditional breather materials, however the inherent texture in these materials produced thickness irregularities that propagated approximately halfway into the thickness of the terminal ply.

The second set of laminates was used to study ply-level imperfections. These laminates were constructed under identical conditions to the first, but their side length was 100 mm. The lamina orientations in each sample were chosen based on the particular imperfection to be examined. An eight-ply $[0°/45°/-45°/90°]_s$ laminate was used to study misalignments in ply orientation as the increased number of plies allowed for a greater number of measurements. Four-ply $[0°/90°]_s$ laminates were used to study variations in ply thickness and thermal gradients. A single laminate was constructed for each type of imperfection studied.

The laminates were vacuum bagged and autoclave cured at a temperature of 120 °C for 2 h according to the specifications of the manufacturer. An external pressure of 80 psi was applied once the laminate reached a temperature of 80 °C. At this point, a dwell time of ~20 min was implemented to allow the resin to reduce in viscosity before applying the pressure. The rate of loading and unloading were 2 °C/min and 3 psi/min for the temperature and pressure profiles, respectively.

3.2. Shape error measurements

The cured shapes of the three 250 mm square samples were measured using a speckle photogrammetry system from Correlated Solutions [29]. Speckle photogrammetry is a technique used to obtain full-field, non-contact measurements of a surface. Fig. 2 shows a picture of the apparatus. Two 5.0 megapixel cameras

Table 1
Orthotropic properties of unidirectional T800 carbon fibers embedded in ThinPreg™120EPHTg-1 epoxy ($V_f \approx 50\%$).

Property	Value
E_1 (GPa)	127.9
E_2 (GPa)	6.5
G_{12} (GPa)	7.5
ν_{12}	0.35
α_1 (ppm/°C)	0.0
α_2 (ppm/°C)	20.0

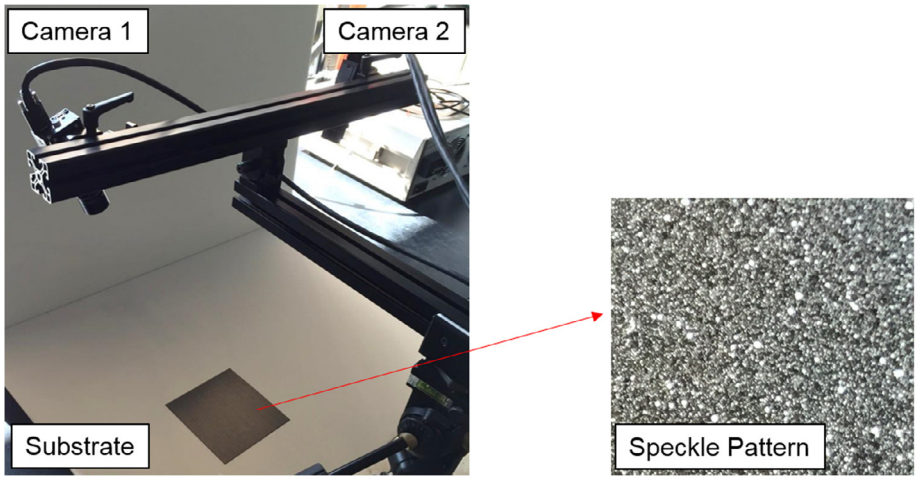

Fig. 2. Speckle photogrammetry apparatus used to measure the shape of the laminates.

(PointGrey GRAS-50S5M-C) with Schneider Cinegon lenses with a 12.7 mm focal length were positioned approximately 0.75 m above the sample. The cameras were offset and angled at ~25° with respect to each other in order to capture stereoscopic images of the sample. An encoded calibration target is used to provide a common reference frame between the two cameras prior to each experiment. The samples were covered with white speckles using matte-finish spray paint, providing a high-contrast pattern against the inherent black surface of the laminate. As this pattern is random in nature, it provides a unique gray-scale signature that varies spatially. The software package, Vic3D, matches this signature between the two cameras across a user-defined grid on the laminate surface, thus determining the coordinates of each grid centroid. By performing this correlation over the entire surface, a full three-dimensional map of the laminate shape is then determined. A 19×19 pixel grid size was used for the measurements, corresponding to an in-plane sampling distance of approximately 2.5 mm. An out-of-plane accuracy of approximately 4 μm was achieved over the 250 mm square. The measurements were conducted with the laminates lying on a flat surface, and thus subject to gravity effects. Attempts were made to conduct measurements in other orientations (i.e. hanging the sample vertical), however the high flexibility of the thin laminates introduced unwanted errors. The measurements were performed approximately 24 h after the completion of the cure. One of the three samples was remeasured 7 days after its cure cycle and no appreciable change in shape was observed.

Fig. 3 displays the measured shapes of the central 225×225 mm^2 portion of each sample; the edge regions were removed to eliminate unwanted measurement-based artifacts. From the measurements it is apparent that significant post-cure shape errors are present. The samples are not flat, as intended by using a flat mandrel and symmetric laminate orientation. The errors are dominated by cylindrical modes oriented in the y-direction. Slight twisting modes are also observed within each sample, the most pronounced associated with Sample 3. The peak-to-valley amplitude of the deformations is approximately 6.0 mm (5.91–6.32 mm) which is ~75 times the thickness of the laminate. Since the deformations differ in shape, it is often convenient to report the root-mean-square (RMS) deviation from a flat surface, d. For m, equally spaced measurements this is defined as

$$d = \sqrt{\sum_{i=1}^{m} w_i^2} \tag{16}$$

where w_i are the grid measurements across the surface after removing the mean and linear (slope) terms in the x and y directions. The RMS shape errors are listed in Fig. 3 for each sample and range from 1.07 to 1.41 mm.

3.3. Characterization of imperfections

3.3.1. Ply misalignments

Optical techniques were used to measure the fiber orientation of the individual plies for one of the 100 mm edge length samples. To measure the fiber orientation, the sample was laid flat and fixed to a precision translation stage. A Nikon ShuttlePix P-400R digital microscope at 400× total magnification (800 μm field of view) was used to capture in-plane images of the laminate surface, revealing the individual fibers within the ply. Image analysis techniques were then used to measure the angles of these fibers with respect to the microscope reference frame. Multiple images were

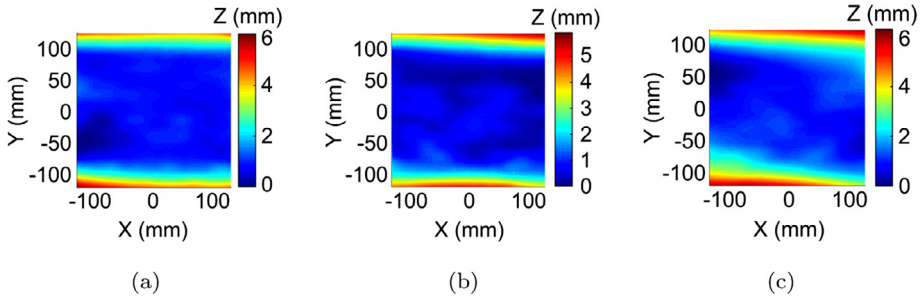

Fig. 3. Measured shape errors of three test samples. (a) Sample 1, d = 1.04 mm, (b) Sample 2, d = 1.16 mm, (c) Sample 3, d = 1.41 mm.

captured at approximately regularly spaced intervals and the mean fiber angle was calculated.

The external plies are initially the only ones accessible for imaging. To expose the internal plies, the laminate was manually polished down in the through-thickness direction until the interface of the next ply was reached at which point images of the second ply were taken. This operation was then performed again at different in-plane locations and through-thickness depths such that each successive ply within the laminate was exposed. An 8-ply $[0°/45°/-45°/90°]_s$ laminate was used for this study and 4 plies were imaged. All measurements were performed with the laminate continually fixed to the stage in order to maintain a constant coordinate system.

The following image analysis techniques were used to extract the fiber angles. Each image was first converted to binary (black and white) using a thresholding value in order to isolate individual fibers from their neighbors based on changes in intensity. Regions along a fiber are assigned a value of 1, while those in between fibers are assigned a value of 0. A Hough Transform [30] was then used to detect straight features within the image, corresponding to the individual continuous fibers. In this technique, lines are parametrically described by:

$$r = x\cos(\alpha) + y\sin(\alpha) \tag{17}$$

where r is the distance measured along a vector perpendicular to the line and intersecting the origin, (i.e. bottom left corner of the image), α is the angle between the r vector and the positive x-axis (ie. bottom of the image), and x and y are the Cartesian coordinates within the image. In this parameterization, lines with equal α values are parallel to one another, while lines containing equal r values are at the same perpendicular distance from the origin. A schematic of this parameterization is shown in Fig. 4.

The transform operates as follows. A matrix, denoted as the accumulator matrix, is first created with rows and columns corresponding to r and α values, respectively. The number of rows/-columns in this matrix are defined by the range and incremental values of r and α to be considered. All entries in the accumulator matrix are initialized at zero at the beginning of the analysis. Then, for every non-zero pixel in the image, individual values of r are calculated for each successive α increment. These r values are rounded off to their nearest increment and the corresponding entries in the accumulator matrix are increased by one. In this fashion, the counts within the accumulator matrix are the number of pixels that have the same (r, α) parameterization. Local maxima within the accumulator matrix correspond to features that have the strongest parameterization and are therefore good candidates for continuous fibers. The orientation of the detected fibers can then be defined as $\beta = \alpha - 90°$.

For this study, the Hough Transform was implemented using MATLAB 6.12 and the built-in functions *hough*, *houghpeaks*, and *houghlines* in order to produce the accumulator matrix, identify the corresponding peaks, and output the detected lines with their corresponding angles in the image coordinate system. A number of parameters can be varied within these functions. Minimum line lengths can be defined, ensuring only continuous fibers are detected. Additionally, closely-spaced neighbors can be ignored by specifying a minimum separation distance between peaks in the accumulator matrix, providing a better spatial distribution of the measured fiber angles across the entire image. Fig. 5 displays an imaged ply along with the lines detected using the Hough Transform. A minimum line length of 1/3rd the image width was defined for the purposes of this study. For each ply, a total of 250–270 fiber angle measurements were performed from 15 individual images.

Fig. 6 displays the measured fiber distributions for each ply along with the mean and standard deviations in fiber angle. It can be seen that the measured fiber angles follow an approximate normal distribution for each ply with standard deviations ranging from 1.9° to 2.2°. The mean of each ply measurement was transformed such that the top 0° ply was taken as a reference orientation. By comparing the measured laminate orientation to the intended orientation, it was found that the plies were oriented to an accuracy of approximately 0.3° for this laminate.

3.3.2. Thickness variations

Ply thickness measurements were made from micrographs of the cross-section of another sample. The sample was first potted in clear casting epoxy and then lapped down using a series of grinding wheels. It was then polished to a smooth surface finish which allowed the ply interfaces as well as individual fibers to be imaged. The micrographs were captured using a Nikon LV-150 optical microscope with a 50× objective lens.

Fig. 7 is a micrograph of a four-ply $[0°/90°]_s$ sample oriented with the 0° fiber direction out of the plane. The bottom ply (Ply 4) corresponds to the ply that was directly in contact with the glass plate during cure. The thickness of the outer plies (Ply 1 and Ply 4) were defined as the distance from the CFRP resin/ potting epoxy interface to the internal 90° fibers. It was not possible to distinguish the interface between the internal plies (Ply 2 and Ply 3) and therefore they were grouped together in one measurement. The combined thickness of these plies was defined as the distance between the top and bottom fibers in the 90° direction. It was then assumed that the thickness of each internal ply was half of the measured value.

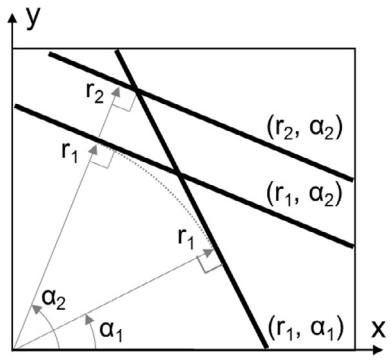

Fig. 4. Schematic of line parameterization used for Hough Transform.

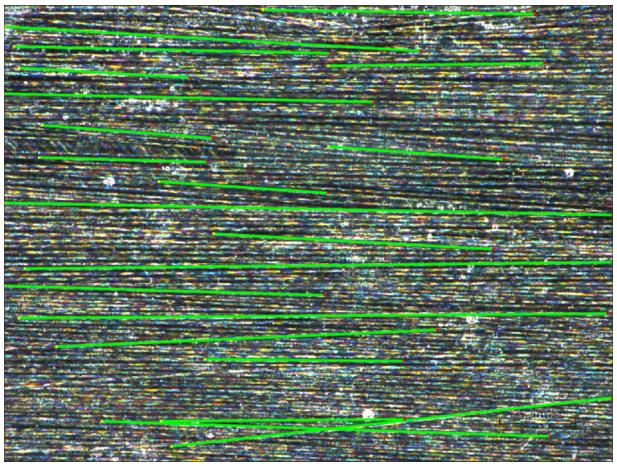

Fig. 5. Image of line detection algorithm used to perform fiber measurements.

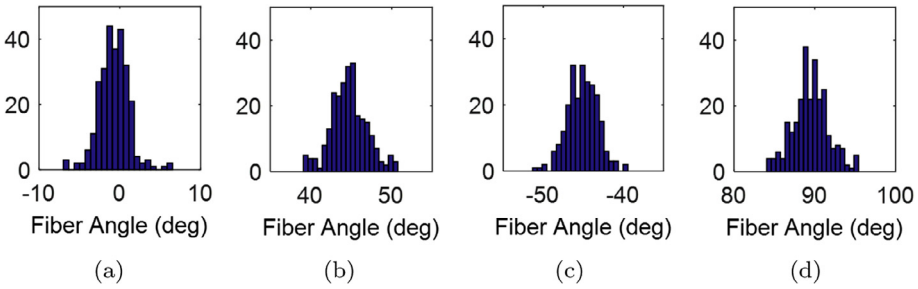

Fig. 6. Fiber angle distribution for Plies 1–4 with mean and standard deviations (μ, σ) of (a) 0.0° (ref), 1.9°, (b) 45.3°, 2.2°, (c) −44.7°, 1.9°, (d) 90.2°, 2.2°.

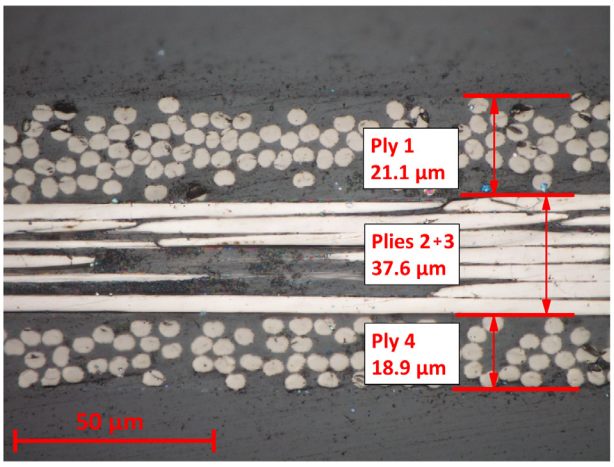

Fig. 7. Micrograph of laminate cross-section displaying ply thickness measurements.

A series of measurements were performed at 2 mm intervals along a 40 mm wide section of the test sample (21 measurements per ply). Table 2 summarizes these measurements in terms of their mean and standard deviation. A significant variation in mean thickness is observed, ranging from 17.8 µm for the inner plies to 21.1 µm for Ply 1. On average, the bottom ply is thinner than the top-ply by 1.3 µm for this specific laminate. An average standard deviation of 2.3 µm was observed over all plies, corresponding to 12% of the average ply thickness.

3.3.3. Thermal gradients during cure

The uniformity of the temperature conditions during cure was assessed by mounting four thermocouples on an additional four-ply $[0°/90°]_s$ test laminate. The thermocouples were placed on either side of the laminate at two locations, as shown in Fig. 8a. Fig. 8b displays the thermal profile during cure with a detailed view of the constant-temperature "soak" section. The temperature was kept relatively constant throughout this section, with only slight variations observed due to the autoclave control cycle.

From this study it is apparent that the mandrel-side of the part is at a higher temperature at both thermocouple locations. A maximum through-thickness temperature change of approximately 0.5 °C was measured between thermocouples 3 and 4. Due to this increased cure temperature, the mandrel-side of the part will be subject to a higher degree of cooling once the part is cooled down to room temperature. While this is a relatively small change in temperature, it represents a large thermal gradient due to the small thickness of the laminate (~6 °C/mm). An in-plane temperature variation of approximately 1 °C was measured across the 100 mm width of the laminate. Therefore, the in-plane thermal gradient is of much lower magnitude (~0.01 °C/mm).

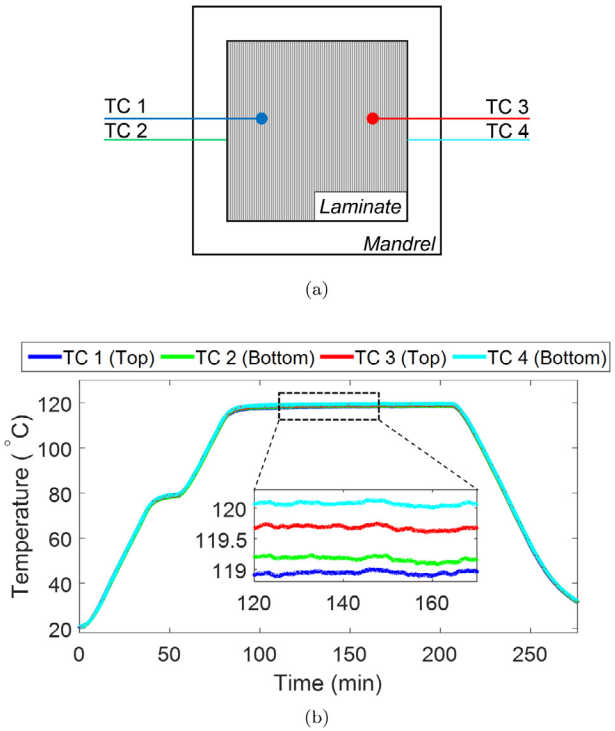

Fig. 8. (a) Schematic of thermocouple placement on laminate. (b) Thermocouple readings during autoclave cure.

Table 2
Ply thickness measurements.

Ply	Mean (µm)	Std. Dev. (µm)
1	21.1	2.6
2 + 3	17.8	2.0
4	19.8	2.2
Avg	19.6	2.3

4. Shape error predictions

The CLT formulation developed in Section 2 was useful in identifying the main effects that cause shape errors. However, it is limited by the assumption of geometric linearity. This is especially true for very thin laminates, as deflections much greater than the thickness have been observed in Section 3.2. To eliminate this assumption, a geometrically non-linear finite element model was created to analyze the effect of the above imperfections on post-cure shape errors.

The commercial finite element package, ABAQUS Standard/CAE 6.12 [31], was used to model the composite plate. S4R shell elements were chosen as the thickness of the laminates is much smaller than any in-plane feature. These elements are 4-node, quadrilateral, elastic elements that can accommodate finite strains and transverse shear deformations. Reduced integration elements were chosen in order to decrease the analysis time. The orthotropic material properties of the lamina, presented in Table 1, were defined as the nominal properties of each ply. The laminate orientation was defined using the built-in composite stack lay-up feature for shell elements. A four-ply, $[0°/90°]_s$, 250 mm square flat laminate was modeled and each ply was assigned a nominal thickness of 20 μm. All 6 degrees of freedom were constrained at a single node located at the center of the plate. A uniform element size of 2.5 mm was used, resulting in 10,000 elements in total across the laminate. A test case was performed with a 1.0 mm element size (62,000 elements in total) in order to study mesh convergence, however the results were shown to differ by less than 1%.

A geometrically non-linear, quasi-static analysis was carried out using the NLGEOM option in Abaqus. A nominal uniform temperature change of −100 °C was defined throughout the plate, simulating the cooling process from 120 °C to 20 °C at the end of the cure cycle. This approach makes the same assumptions mentioned in Section 2; however, geometric non-linearities are handled properly by automatic updating of the tangent stiffness matrix throughout the analysis. The size of the analysis increment was allowed to adjust automatically, however a maximum increment of 5 °C was defined for each simulation.

The main output of each analysis is the shape of the laminate after the cool-down process, provided by the nodal deformations in the model. For further characterization, the deformed shape was projected onto a set of quadratic basis functions corresponding to the cylindrical curvatures along the x and y axes, κ_x and κ_y, as well as twist, κ_{xy}. These functions can be assembled into a basis matrix, $\mathbf{P}$, defined as

$$\mathbf{P} = \begin{bmatrix} \frac{1}{2}x_1^2 & \frac{1}{2}x_2^2 & \dots & \frac{1}{2}x_m^2 \\ \frac{1}{2}y_1^2 & \frac{1}{2}y_2^2 & \dots & \frac{1}{2}y_m^2 \\ & & & \\ x_1y_1 & x_2y_2 & \dots & x_my_m \end{bmatrix}^T \tag{18}$$

where x_i and y_i are the in-plane coordinates of the deformed laminate. The least-squares best-fit curvatures and twist are then found using

$$\boldsymbol{\kappa} = \mathbf{P}^{-1}\mathbf{W} \tag{19}$$

where $\boldsymbol{\kappa} = [\kappa_x \ \kappa_y \ \kappa_{xy}]^T$, and $\mathbf{W}$ is a vector containing the coordinates, z_i, of the deformed laminate. In this formulation, positive curvatures correspond to a concave surface oriented in the positive z-direction and a positive twist corresponds to a saddle shape with positive out-of-plane coordinates in the first quadrant of a square laminate.

The following sections present the procedures used to model the three types of imperfections identified in Section 3.3. Comparisons between the non-linear finite element analysis and linear CLT predictions are also made.

4.1. Variations in ply alignment

To model the effect of ply misalignment, the mean orientation of a single ply was varied in the laminate stacking sequence while keeping all other ply angles fixed. Fig. 9a and b display the resulting curvature changes as a function of ply misalignment in the terminal 0° and internal 90° plies, respectively. Fig. 9c displays the corresponding RMS shape error.

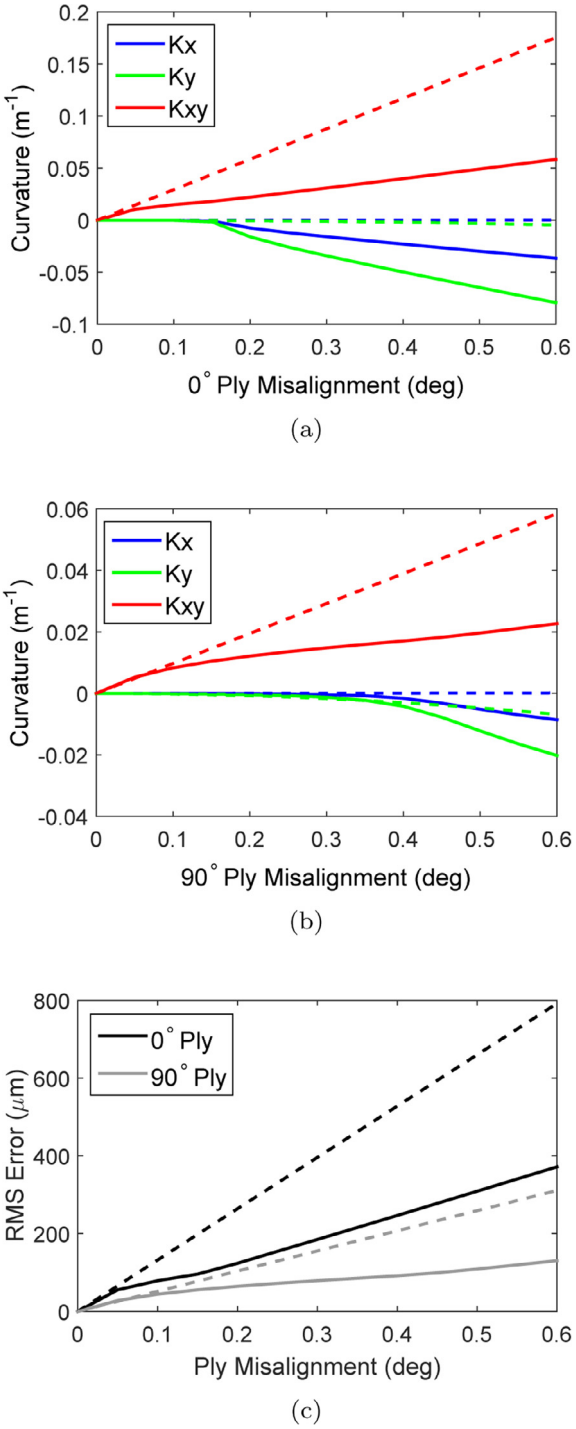

Fig. 9. Results of non-linear FEA (solid) and CLT prediction (dashed) for uniform variations in orientation of one ply due to (a) 0° ply and (b) 90° ply misalignments and (c) the resulting shape error magnitudes.

Several observations can be made from these results. Firstly, by comparing Fig. 9a and b, it is evident that the laminate is more sensitive to variations in the 0° ply orientation in comparison to those for the 90° ply, as the resulting curvatures are larger. This is as expected as the 0° ply is further away from the mid-plane of the laminate, thus producing a larger thermally-induced moment from the imbalance. Second, for both the 0° and 90° plies, at small values of misalignments (<0.05°) there is good agreement between the results of the non-linear finite element analysis and the CLT predic-

tion. Both analyses predict a strong twisting mode of deformation, as κ_{xy} is the only non-zero curvature component. For ply misalignments >0.05° the non-linear results begin to deviate from the CLT prediction and the rate of growth of κ_{xy} declines. Upon further increase of the ply misalignment, the non-linear analysis captures a mode change in the deformation of the laminate as κ_x and κ_y become non-zero. This transition occurs at a misalignment of approximately 0.15° for the 0° ply and 0.35° for the 90° ply. Finally, by studying Fig. 9c it can be seen that these twisting modes and curvature changes result in large magnitude shape errors. The CLT analysis greatly over-predicts the magnitude of shape error during cooling because if does not capture non-linear geometric effects.

The observed differences associated with the geometrically linear CLT analysis and non-linear finite element simulation can be understood by considering the Gaussian curvature change of the laminate. The Gaussian curvature is defined as the product of the principal curvatures, κ_1 and κ_2 [32]:

$$K = \kappa_1 \kappa_2 \tag{20}$$

which are related to the curvatures in the laminate coordinate system by

$$\kappa_{1,2} = \frac{\kappa_x + \kappa_y}{2} \pm \sqrt{\frac{(\kappa_x - \kappa_y)^2}{2} + \kappa_{xy}^2}. \tag{21}$$

Mid-plane stretching is required in order for a change in Gaussian curvature to occur. Therefore, for a flat plate initially having $K = 0$, the mid-plane must stretch if it is to take on a non-zero K configuration. This will occur if the plate deforms with non-zero κ_{xy}, or if both κ_x and κ_y become non-zero. However, if the plate undergoes pure bending in one direction, the Gaussian curvature of the plate will not change and mid-plane stretching is not required.

For thin plates, the strain energy contribution due to membrane stretching is much higher in comparison to that of inextensional bending. For example, if we consider an isotropic plate with modulus, E, Poisson's ratio, ν, and thickness, t, the strain energy per unit area due to pure stretch in one direction is

$$U_m = \frac{Et}{2(1-\nu^2)} \epsilon_m^2 \tag{22}$$

while the strain energy per unit area due to pure bending in one direction is

$$U_b = \frac{Et^3}{24(1-\nu^2)} \kappa_b^2. \tag{23}$$

To compare the relative energy contribution for the two cases the above expressions can be equated to arrive at the following relationship:

$$\kappa_b = \sqrt{12} \frac{\epsilon_m}{t} \tag{24}$$

which provides a method to compare energetically equivalent curvature changes due to inextensional bending, and mid-plane strains due to membrane stretching. For the plate thicknesses associated with this study ($t = 80$ μm), large curvatures would result from equivalent strain energies associated with small mid-plane strains. For example, a membrane strain of only 0.1% would correspond to a curvature change of 4.3 m^{-1} – an extremely large value. Therefore, energetically favorable solutions will often be ones that minimize membrane strains and thus changes in Gaussian curvature.

Fig. 10 displays the Gaussian curvature change as a function of ply misalignment predicted from the CLT analysis and the non-linear finite element simulation. It is apparent that the CLT solutions involve much larger changes in Gaussian curvature than the geometrically non-linear results. The non-linear solutions increase until a local peak in Gaussian curvature is reached and then decrease in magnitude, whereas the CLT solutions increase monotonically. These peaks correspond to the values of ply misalignment associated with the observed mode-changes in Fig. 9a and b.

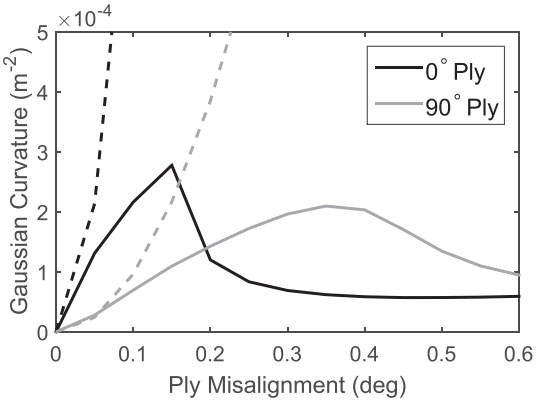

Fig. 10. Gaussian curvature change for non-linear FEA (solid) and CLT prediction (dashed) for uniform variations in ply orientation.

4.2. Uniform variations in ply thickness

Variations in ply thickness were imposed by reducing the thickness of the top 0° ply while keeping the thickness of all other plies equal to the nominal value of 20 μm. Variations in the thickness of the internal 90° plies do not result in shape errors as the laminate remains balanced, and therefore were not considered. The ply thickness variation was carried out in the model by modifying the composite stack lay-up formulation in the shell section definition. It was assumed that the material properties of the modified ply remained constant throughout this process.

Fig. 11 displays the resulting curvature changes and RMS shape error due to uniform changes in the top ply thickness. From Fig. 11a, it is evident that large curvature changes arise even for very small changes in ply thickness. The dominating curvature change occurs in the y-direction, resulting in a cylindrical mode of deformation. A lower magnitude κ_x term of opposite sign is also predicted from the CLT analysis. The relative magnitude of these curvature components can be understood by considering the stacking sequence of the highly orthotropic plies in the laminate. As the top and bottom 0° plies have much higher stiffness along the x-axis, the laminate will have a higher bending stiffness in this direction. As a result, the laminate will be more resistant to imbalances in thermal strains, and ultimately thermal moments, in the x-direction. The sign of the resulting curvatures can be understood by considering the extreme case of removing the top ply altogether, representing a reduction in thickness equal to the nominal ply thickness. In this case, thermal contraction of the 90° plies will cause a positive thermal moment in the x-direction as they react against the bottom ply with zero CTE in that direction. Conversely, thermal contraction of the bottom, 0° ply in the y-direction will cause a negative moment to form, ultimately resulting in a negative κ_y.

There is good agreement between the non-linear finite element analysis and the CLT prediction for κ_y, however the non-linear results show $\kappa_x = 0$ for all studied variations in ply thickness. Therefore, the non-linear results indicate that the laminate will deform in an inextensional bending mode (i.e. $K = 0$ throughout). From Fig. 11b, it can be seen that small changes in ply thickness result in extremely large shape error magnitudes over the

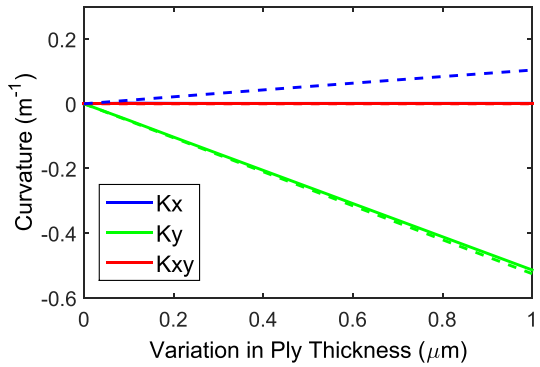

(a)

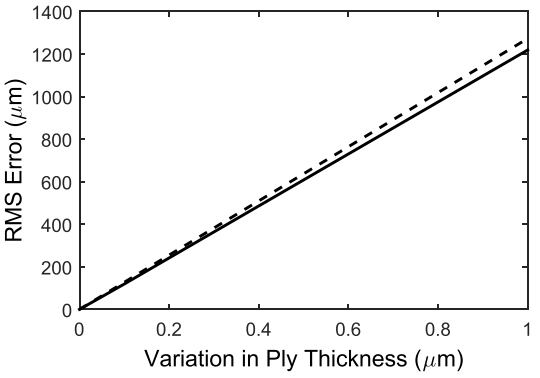

(b)

Fig. 11. Results of non-linear FEA (solid) and CLT prediction (dashed) for uniform variations in 0° ply thickness. (a) Laminate curvatures and (b) resulting shape error magnitudes.

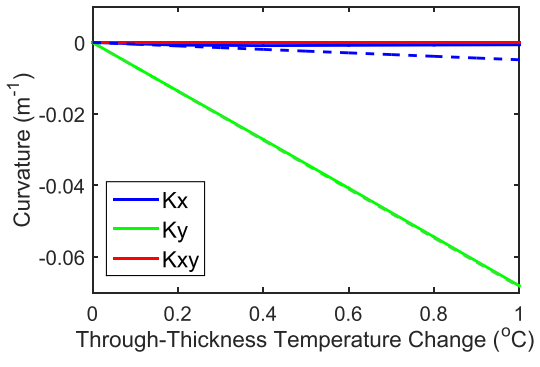

(a)

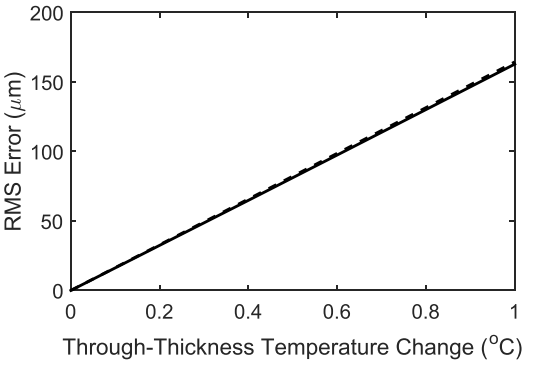

(b)

Fig. 12. Results of non-linear FEA (solid) and CLT prediction (dashed) for thermal gradients during cure. (a) Laminate curvatures and (b) resulting shape error magnitudes.

250 mm square plate. The growth of shape error is linear with respect to changes in ply thickness.

4.3. Through-thickness thermal gradients

Finally, the shape errors produced as a result of through-thickness thermal gradients were studied. In this study, the temperature change of the shell mid-plane was set to the nominal value of −100 °C as before, however a linear variation through the thickness was also defined to simulate a through-thickness gradient in cure temperature. In this analysis, a negative thermal gradient was defined such that the bottom surface experienced a higher degree of cooling than the top, as observed in practice (see Section 3.3.3).

The results of this analysis are shown in Fig. 12. It can be seen that the through-thickness temperature change produces a negative-sense cylindrical deformation oriented in the y-direction as κ_y is the dominating curvature term. A very small negative component of κ_x is predicted by the CLT analysis, however this is not present in the non-linear finite element analysis, indicating an inextensional bending mode of deformation. The agreement between the CLT prediction and the non-linear analysis is apparent in the magnitude of predicted shape error, shown in Fig. 12b.

4.4. Sensitivity analysis

In order to compare the relative effect of each imperfection, it is necessary to normalize their magnitudes. Two methods of normalization were considered: normalization by the full-scale value of each imperfection, and normalization by the measured values presented in Section 3.3. The full-scale values were taken to be (1) the difference between the external/internal ply orientations, (2) the total ply thickness, and (3) the full temperature change experienced during cure. The measured values were defined as (1) the maximum deviation in measured ply orientation, (2) the difference in thickness between the top and bottom plies, and (3) the through-thickness difference in temperature measured during cure. Table 3 lists these values for the three types of imperfections considered.

Fig. 13a displays the influence of each imperfection as a fraction of its full-scale value, showing results that were obtained using the non-linear finite element analysis. This plot is useful from a design standpoint if no a priori knowledge of the imperfection magnitudes is available. From the plot it is clear that the alignment of the 0° ply is the dominating imperfection, resulting in an RMS error of approximately 550 μm at 1% of the full-scale value. The remaining imperfections have similar but reduced sensitivity, resulting in approximately 200 μm of deformation at their respective 1% magnitudes.

Fig. 13b displays the influence of each imperfection as a fraction of the measured values. This plot provides insight into the level of

Table 3
Full-scale and measured values of imperfections.

Imperfection	Full-scale	Measured
Ply misalignment (deg)	90.0	0.3
Ply thickness variation (μm)	20.0	1.3
Through-thickness ΔT (°C)	100.0	0.5

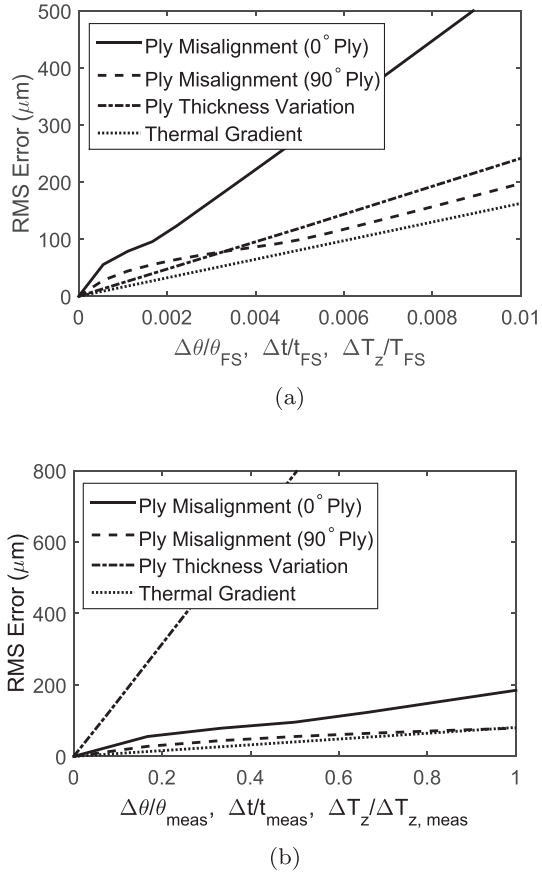

Fig. 13. RMS error as a function of imperfection magnitude. Results are normalized by (a) the full-scale (FS) values and (b) the measured (meas) values in Table 3.

shape error reduction that can be achieved if the magnitude of imperfections were to decrease from the current measured values. From this analysis it can be seen that the variation in ply thickness is clearly the dominant factor. The deformation of the laminate is extremely sensitive to variations in this parameter with out-of-plane deformations in excess of 1500 μm RMS.

4.5. Comparison to experiments

For comparative purposes, the measured levels of imperfection were injected into the non-linear finite element model and shape error predictions were made in three separate analyses. The orientation and mean thickness variations were modeled as random variables as no systematic behaviors had been observed. Misalignments in the orientation of each ply were assumed to follow a zero-mean, normal distribution with a standard deviation of 0.3°. Ply thickness variations were implemented by increasing the thickness of the top ply while keeping all others constant. This variation was assumed to follow a uniform distribution on the interval [0, 1.3 μm], ensuring that the top ply always increased in thickness. The through-thickness temperature variation was held constant at −0.5 °C for all three analyses. Table 4 displays the values used for these simulations.

Table 4
Imperfection magnitudes used for comparison to experiments.

Imperfection	Modeled parameters
Ply Misalignment	$\Delta\theta \sim \mathbf{N}(0, 0.3°)$
Ply Thickness Variation	$\Delta t_{top} \sim \mathbf{U}[0, 1.3\ \mu m]$
Through-Thickness ΔT	$\Delta T_z = -0.5\ °C$

Fig. 14 displays the shape errors predicted by the three simulations using the imperfections listed in Table 4. The results are shown for the central 225 × 225 mm^2 portion of the model, as it had been done for the experimental results. The model predicts dominating curvature terms oriented in the *y*-direction, similar to those observed in the measurements from Section 3.2. A slight twisting component is obtained from Analyses 1 and 2, however it is less pronounced in Analysis 3.

These three analyses correspond to higher magnitude shape errors than those obtained from the experiments. Peak-to-valley amplitudes ranging from 6.8 to 8.1 mm (1.62 to 2.37 mm RMS) are predicted whereas the experiments gave values of 5.91 to 6.32 mm (1.07 to 1.41 mm RMS). It should be noted that gravity effects were not included in the finite element model as it would be difficult to define the proper boundary conditions for accurate experimental comparison. For example, during the measurements the cured laminates were laid flat on a table and allowed to drape along its surface. Implementation of this effect in the finite element model would require contact formulations to be established, adding a significant level of complexity.

5. Discussion and conclusion

The post-cure shape errors associated with nominally symmetric thin-ply composite laminates have been studied. The study focused on shape errors of four-ply $[0°/90°]_s$ laminates with 20 μm thick plies. Full-field shape measurements were performed for three samples that had been cured at elevated temperatures and then cooled to room temperature. Significant curvature and twisting-based deformations were observed with maximum out-of-plane displacements on the order of 75 times the laminate thickness.

Three types of imperfections associated with thin-ply laminates were studied using small-scale samples that were fabricated under identical conditions: (1) misalignments in ply orientation, (2) variations in ply thickness, and (3) through-thickness thermal gradients. Deviations in ply angles were measured from images taken with a digital microscope. The laminate was lapped down in the through-thickness direction in order to image the internal ply orientations. By comparing the actual orientation of the plies to the intended laminate orientation, it was found that the mean angle error was approximately 0.3°. Ply thickness uniformity was measured from micrographs of a laminate cross-section. The ply in contact with the mandrel surface during cure was found to be thinner than that on the top by 1.3 μm, or 6.5% of the nominal ply thickness. Finally, the through-thickness variation in the cure temperature was measured by equipping a laminate with thermocouples. A 0.5 °C through-thickness difference in temperature was observed with the mandrel side of the part at higher temperatures than the top.

Through non-linear finite element simulations, it was shown that each of these imperfections results in post-cure shape errors upon cooling from the elevated cure temperature. It was found that Classical Lamination Theory is inaccurate in predicting the mode and magnitude of imperfection-induced deformations, especially for imperfections that induce large changes in Gaussian curvature. Ply misalignments tended to produce twisting modes of deformation, while variations in ply thickness and through-thickness thermal gradients caused the laminate to deform in an inextensional bending mode.

A sensitivity analysis was performed in order to identify the imperfection with the greatest influence on shape errors. Variations in ply thickness were shown to be the most relevant when

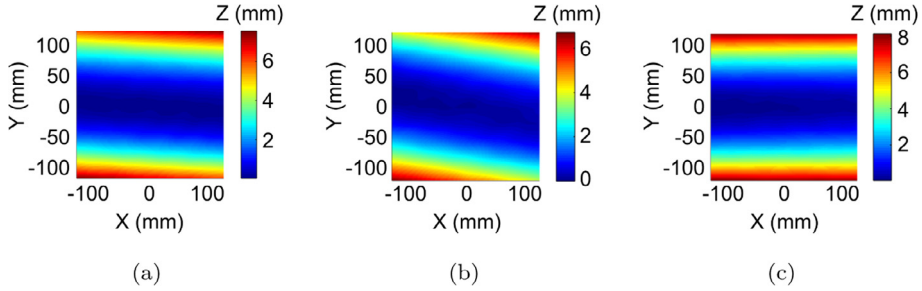

Fig. 14. Simulated shape errors resulting from measured imperfection magnitudes. (a) Analysis 1, d = 2.07 mm, (b) Analysis 2, d = 1.62 mm, (c) Analysis 3, d = 2.37 mm.

taking into account the observed magnitude of imperfections. However, as the number of plies was limited at four for this study, investigation into whether this result would extend to laminates with higher ply counts should be performed.

Finally, three separate analyses were performed for experimental comparison by injecting the level of measured imperfections into the finite element model. Similar modes of deformation were observed although 68% larger amplitudes were predicted in comparison to the experiments when considering the RMS surface deviation from a flat. Additionally, the results of the finite element simulations indicate that the studied imperfections result in smooth curvature and twisting modes of deformation. However, in studying the shape of the measured imperfections, it was also apparent that the post-cure errors are not necessarily limited to these global modes. In fact, several shorter wavelength surface features are also observed, indicating the need for further investigation into spatially variant imperfections across the surface of the laminates.

Acknowledgments

Financial support from the Natural Sciences and Engineering Research Council (NSERC) of Canada is gratefully acknowledged. A part of this research was carried out at the Jet Propulsion Laboratory, California Institute of Technology under a contract with the National Aeronautics and Space Administration (NASA).

References

[1] Tsai SW, Sihn S, Kim RY. Thin ply composites. JEC-Compos 2005;18:31–3.
[2] EL-Dessouky HM, Lawrence CA. Ultra-lightweight carbon fibre/thermoplastic composite material using spread tow technology. Compos Part B: Eng 2013;50:91–7.
[3] North thin ply technologies, <http://www.thinplytechnology.com/; 2014.>
[4] Sihn S, Kim RY, Kawabe K, Tsai SW. Experimental studies of thin-ply laminated composites. Compos Sci Technol 2007;67(6):996–1008.
[5] Yokozeki T, Aoki Y, Ogasawara T. Experimental characterization of strength and damage resistance properties of thin-ply carbon fiber/toughened epoxy laminates. Compos Struct 2008;82(3):382–9.
[6] Yokozeki T, Kuroda A, Yoshimura A, Ogasawara T, Aoki T. Damage characterization in thin-ply composite laminates under out-of-plane transverse loadings. Compos Struct 2010;93(1):49–57.
[7] Amacher R, Cugnoni J, Botsis J, Sorensen L, Smith W, Dransfeld C. Thin ply composites: experimental characterization and modeling of size-effects. Compos Sci Technol 2014;101:121–32.
[8] Mallikarachchi H, Pellegrino S. Design of ultrathin composite self-deployable booms. J Spacecraft Rockets 2014;51(6):1811–21.
[9] Brinkmeyer A, Pellegrino S, Weaver PM. Effects of long-term stowage on the deployment of bistable tape springs. J Appl Mech 2016;83(1):011008.
[10] Rimrott F. Storable tubular extendible member: a unique machine element. Mach Des 1965;37(28):156–65.
[11] Murphey TW, Banik J, Triangular rollable and collapsible boom, US Patent 7,895,795 (Mar. 1 2011).
[12] Steeves J, Laslandes M, Pellegrino S, Redding D, Bradford SC, Wallace JK, Barbee T. Design, fabrication and testing of active carbon shell mirrors for space telescope applications. SPIE astronomical telescopes+ instrumentation. International Society for Optics and Photonics; 2014. p. 915105–915105.
[13] Chen PC, Romeo RC. Fabrication and testing of very lightweight composite mirrors. Astronomical telescopes & instrumentation. International Society for Optics and Photonics; 1998. p. 938–45.
[14] Hinckley M. Statistical evaluation of the variation in laminated composite properties resulting from ply misalignment 1990. http://dx.doi.org/10.1117/12.21532.
[15] Arao Y, Koyanagi J, Utsunomiya S, Kawada H. Effect of ply angle misalignment on out-of-plane deformation of symmetrical cross-ply cfrp laminates: accuracy of the ply angle alignment. Compos Struct 2011;93(4):1225–30.
[16] Kratmann KK, Sutcliffe M, Lilleheden L, Pyrz R, Thomsen OT. A novel image analysis procedure for measuring fibre misalignment in unidirectional fibre composites. Compos Sci Technol 2009;69(2):228–38.
[17] Yurgartis S. Measurement of small angle fiber misalignments in continuous fiber composites. Compos Sci Technol 1987;30(4):279–93.
[18] Kyriakides S, Arseculeratne R, Perry E, Liechti K. On the compressive failure of fiber reinforced composites. Int J Solids Struct 1995;32(6):689–738.
[19] Knibbs R, Morris J. The effects of fibre orientation on the physical properties of composites. Composites 1974;5(5):209–18.
[20] Berthelot J. Effect of fibre misalignment on the elastic properties of oriented discontinuous fibre composites. Fibre Sci Technol 1982;17(1):25–39.
[21] Jortner J. A model for predicting thermal and elastic constants of wrinkled regions in composite materials. Eff Defects Compos Mater 1984:217–36.
[22] Karami G, Garnich M. Micromechanical study of thermoelastic behavior of composites with periodic fiber waviness. Compos Part B: Eng 2005;36 (3):241–8.
[23] Arao Y, Koyanagi J, Utsunomiya S, Kawada H. Time-dependent out-of-plane deformation of ud-cfrp in humid environment. Compos Sci Technol 2009;69 (11):1720–5.
[24] Bogetti TA, Gillespie JW. Process-induced stress and deformation in thick-section thermoset composite laminates. J Compos Mater 1992;26(5):626–60.
[25] Antonucci V, Giordano M, Hsiao K-T, Advani SG. A methodology to reduce thermal gradients due to the exothermic reactions in composites processing. Int J Heat Mass Transfer 2002;45(8):1675–84.
[26] Jones RM. Mechanics of composite materials. CRC Press; 1998.
[27] Twigg G, Poursartip A, Fernlund G. Tool–part interaction in composites processing. part i: experimental investigation and analytical model. Compos Part A: Appl Sci Manuf 2004;35(1):121–33.
[28] Twigg G, Poursartip A, Fernlund G. Tool–part interaction in composites processing. part ii: numerical modelling. Compos Part A: Appl Sci Manuf 2004;35(1):135–41.
[29] Correlated solutions, <http://www.correlatedsolutions.com/>; 2014.
[30] Hough PV, Method and means for recognizing complex patterns, US Patent 3,069,654 (Dec. 18 1962).
[31] Abaqus CAE/Standard 6.12, Simulia Inc., Providence, RI (2012).
[32] Calladine CR. Theory of shell structures. Cambridge University Press; 1989.